LEI WANG
YAO WEI
and
YONGYI REN

# Instability analysis of anchorage supporting in soft rock roadways based on strain softening

*In view of the problems such as spray layer peeling-off, reduced anchoring force and serious floor heave in the weakly cemented soft rock roadway in the west region, we took samples from the sandy mudstone formation in the main haulage roadway of Luxin Coal Mine in Inner Mongolia and performed triaxial compression tests at different confining pressure in the lab. The test data show that the post-peak strain behaviour of the mudstone is obviously softened and there exists residual deformation, thus the tri-linear strain-softening model is more suitable for analysis. We made fish corrections to the bi-linear strain-softening model in FLAC to achieve the numerical application of the model. The verification model shows that the tri-linear strain-softening model better describes the deformation features of mudstone. We analyzed the construction stability of the mudstone roadway and conducted evaluation based on the softening index. The results show that due to the increasing softening degree and softening depth of the mudstone roadway, the shotcreting support system has no obvious effect in controlling the deformation of the surrounding rock, and that the bolt axial force first increases and later decreases, losing its retaining effect.*

***Keywords:*** *Weakly cemented mudstone, triaxial compression, strain softening, degree of softening, numerical simulation.*

## 1. Introduction

In many mining areas in West China, the roofs and floors of the roadways are made of low-strength, weakly cemented mudstone, sandstone and other Jurassic soft rock. The poor self-bearing capacity makes roadway support very difficult, leading to problems like spray layer peeling-off, reduced anchor force and severe floor heave. The reasons are as follows: 1. The roof and floor rocks have very low strength and poor bearing capacity and the formation load is mainly borne by the supporting structure; 2. Anchor bolts do not match the surrounding rocks – the anchor bolts and adhesive bonds have high strength while the surrounding rock has low strength, resulting in the separation of the bonds from the surrounding rocks and further causing anchor support failures [1-2]. Therefore, it is important to study the mechanical properties of such soft rocks [3-4], especially their post-peak strain behaviour. It is of great value to the research on the loss of anchorage force and the instability of supporting structure in soft rock roadways.

In view of this soft rock engineering problem, Li Dongwei et al. [5-6] carried out an indoor rheological test on soft rock, analyzed its creep deformation characteristics, and described the constitutive relations of such rocks; Lu Yinlong [7] carried out an indoor mechanical experiment on soft rock, analyzed its post-peak mechanical behaviour and defined the softening factor to study the softening degree of rock. Zhao Zenghui et al. [8] studied the damage evolution law of western soft rock in the triaxis compression test; Liao Hongjian [9-10] performed a consolidation-undrained shear test on the heavily weathered expansive mudstone and the results showed that the stress-strain curve of the mudstone takes on the feature of strain softening, and this feature of the expansive mudstone is not weakened with the increase of the confining pressure. Meng Qingbin et al. [11-12] systematically studied the mechanical characteristics of Cretaceous and Jurassic weakly cemented soft rock, and proposed a volumetric strain-softening model.

The above research results are of great significance to revealing the mechanic characteristics of the Jurassic soft rock in West China and giving guidance to soft rock roadway support, but the mechanical problems of such soft rock are still in need of further systematic study.

## 2. Tri-axial compression behaviour of typical soft rock

### 2.1 Field sampling

The test area, located 20km northeast of the Wulagai Management Zone of Xilin Gol League, belongs to the Mesozoic Jurassic-Cretaceous coal-bearing tectonic system, hosted in the continental coal-bearing basin controlled by different levels of structures. The coal-bearing stratum is composed of fine conglomerate, coarse sandstone, medium sandstone, fine sandstone, siltstone, mudstone and coal bed. The average depth of the main roadway is 344.45m. The roof

Messrs. Lei Wang and Yao Wei, College of Architecture and Civil Engineering, Xi'an University of Science and Technology, Xi'an 710 054, and Yongyi Ren, Economic and Technical Research Institute, Shandong Electric Power Company State Grid, Jinan 250 000, China. Email: wls3016@163.com

and floor of the coal bed consist of sandy mudstone and siltstone, with an average thickness of 12.07m and 7.49m respectively. The top and the bottom are 12.07m and 7.49m respectively. The test rock samples of the weakly cemented sandy mudstone were taken from the floor of this coal bed.

After we took the rock samples by drilling on site and sent them to the laboratory, we processed and tested them by batch according to the test design. After unpacking the rock samples, we carried out cutting → core boring → end-face grinding, and obtained the processed rock specimens, as shown in Fig.1.

(a) Taking rock samples on site (b) Processed rock specimens

Fig.1 Rock specimens

### 2.2 Analysis of the triaxial compression test

We carried out the triaxial test with the triaxial apparatus developed by Changchun Chaoyang Test Instrument Co., Ltd. and the university at a mudstone confining pressure of 1MPa, 3MPa and 5MPa according to the roadway ground stress test results and the uniaxial test strength, and the test results are shown in Fig.2.

It can be seen from Fig.2 that, under the confining pressure, the deformation behaviour of the weakly cemented mudstone has changed a lot compared to the uniaxial compression results, showing an obvious strain-softening feature.

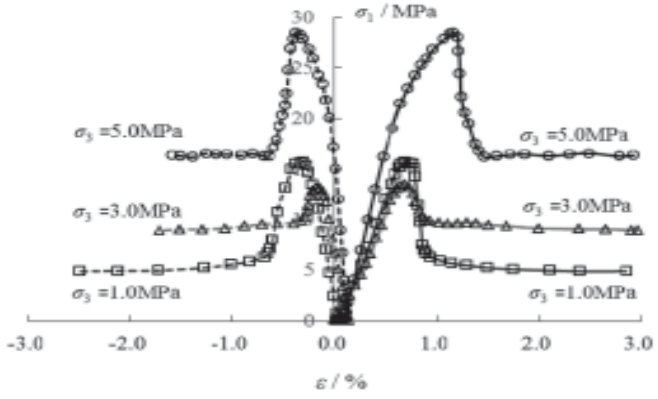


Fig.2 Triaxial compression curve of mudstone

## 3. Generalized strain-softening model

### 3.1 Constitutive relation of the linear strain-softening

At present, the strain-softening model in the FLAC 2D and 3D versions is a simplified broken line type model, which cannot well reflect the deformation characteristics of the rock after the peak stress. Based on the triaxial stress-strain curve of mudstone in Fig.2, this paper adopts the tri-linear strain-softening constitutive relation. The structure is shown in Fig.3.

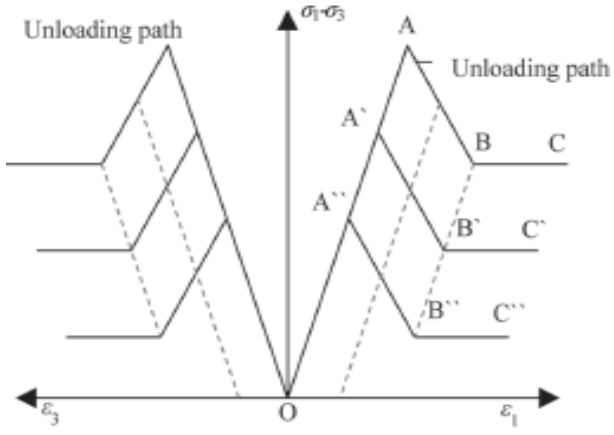


Fig.3 Linear strain-softening model

Since the weakly-cemented mudstone is subjected to irreversible plastic deformation after being loaded, the deformation of the mudstone under load can be expressed as the sum of elastic deformation and irreversible plastic deformation, that is:

$$\varepsilon_{ij} = \varepsilon_{ij}^{e} + \varepsilon_{ij}^{p} \quad \ldots \quad 1)$$

With the impact of the intermediate principal stress ignored, the plastic strain value is only related to the corresponding maximum principal stress and minimum principal stress. According to the strain theory, the plastic shear strain can be expressed as:

$$\varepsilon^{ps} = \frac{1}{\sqrt{2}}\sqrt{(\varepsilon_1^p - \varepsilon_m^p)^2 + (\varepsilon_m^p)^2 + (\varepsilon_3^p - \varepsilon_m^p)^2} \quad \ldots \quad (2)$$

$$\varepsilon_m^p = \frac{1}{3}(\varepsilon_1^p + \varepsilon_3^p) \quad \ldots \quad (3)$$

As we need to consider the effect of plastic shear strain, the internal friction angle and internal cohesion of the rock in the Mohr-Coulomb theory are no longer constant values, but the variables related to the plastic shear strain; in other words, the rock internal friction angle $\varphi$ and the internal cohesion c can be expressed as generalized cohesion $\bar{c}(\sigma,\varepsilon^{ps})$ and generalized friction angle $\bar{\varphi}(\sigma, \varepsilon^{ps})$ [13-14], so the yield function can be expressed as:

$$f = \sigma_1 - \sigma_3 \cdot \frac{1+\sin\bar{\varphi}(\sigma,\varepsilon^{ps})}{1-\sin\bar{\varphi}(\sigma,\varepsilon^{ps})} + 2\cdot\bar{c}(\sigma,\varepsilon^{ps})\sqrt{\frac{1+\sin\bar{\varphi}(\sigma,\varepsilon^{ps})}{1-\sin\bar{\varphi}(\sigma,\varepsilon^{ps})}} \quad \ldots \quad (4)$$

According to the triaxial compression curve of mudstone in Fig.2, the generalized cohesion $\bar{c}(\sigma,\varepsilon^{ps})$ and the generalized friction angle $\bar{\varphi}(\sigma, \varepsilon^{ps})$ under different plastic

Table 1: Generalized internal cohesion of mudstone

| $\varepsilon^{ps}/10^{-3}$ | Generalized internal cohesion /MPa | | | |
|---|---|---|---|---|
| | Confining pressure 0 MPa | Confining pressure 1 MPa | Confining pressure 3 MPa | Confining pressure 5 MPa |
| 0 | 1.31 | 1.52 | 2.08 | 2.56 |
| 5.0 | 1.16 | 1.31 | 1.82 | 2.31 |
| 10.0 | 0.91 | 1.02 | 1.59 | 2.02 |
| 15.0 | 0.63 | 0.81 | 1.32 | 1.76 |
| 20.0 | 0.36 | 0.62 | 1.06 | 1.47 |

Table 2: Generalized internal friction angle of mudstone

| $\varepsilon^{ps}/10^{-3}$ | Generalized internal friction angle $\overline{\varphi}$ /° | | | |
|---|---|---|---|---|
| | Confining pressure 0 MPa | Confining pressure 1 MPa | Confining pressure 3 MPa | Confining pressure 5 MPa |
| 0 | 19.8 | 19.32 | 18.76 | 17.64 |
| 5.0 | 18.77 | 18.42 | 18.07 | 16.79 |
| 10.0 | 17.98 | 17.64 | 17.31 | 16.03 |
| 15.0 | 17.22 | 16.92 | 16.45 | 15.37 |
| 20.0 | 16.52 | 16.03 | 15.71 | 14.85 |

strains can be obtained. The calculation results are shown in Tables 1 and 2.

From the results of generalized internal cohesion and generalized internal friction angle listed in Tables 1 and 2, we can obtain the relationships between the generalized cohesion and the generalized friction angle $\overline{\varphi}$ and the confining pressure $\sigma_3$ and plastic shear strain $\varepsilon^{ps}$ by fitting, as expressed in the following formulas:

... (5)

$$\overline{\varphi} = \begin{bmatrix} (\sigma_3)^3 \\ (\sigma_3)^2 \\ (\sigma_3)^1 \\ 1 \end{bmatrix} \begin{bmatrix} 0 & 0 & 0 & 0 \\ 0 & 0 & 0.0002 & 0.0002 \\ 0 & 0 & 0.0009 & -0.068 \\ 0 & 0.0008 & 0.1662 & 19.231 \end{bmatrix} \begin{bmatrix} (\varepsilon^{ps})^3 \\ (\varepsilon^{ps})^2 \\ (\varepsilon^{ps})^1 \\ 1 \end{bmatrix} \quad \text{... (6)}$$

3.2 Implementation and verification of the strain-softening model in FLAC3D

The strain-softening model embedded in FLAC3D is a bi-linear model. In the FLAC, the stress-strain correction is made to the embedded SS model based on the incremental plastic strain-stress relationship to realize the application of this model. Specific steps are as follows: when the element is in the elastic state, the strain increment is directly calculated by the SS model according to the generalized Hooke law; when the element gets into the plastic strain state, the stress increment is determined by the minimum principal stress and the current strain state. After the stress is updated, the strain increment will be reanalyzed. The process can be directly achieved by the fish programming in the FLAC3D, so we will not elaborate more on this.

In order to verify the applicability of this model, we built a numerical model to perform compression test at 0MPa (i.e. uniaxial compressive strength), 1MPa, 3MPa and 5MPa, as shown in Fig.4.

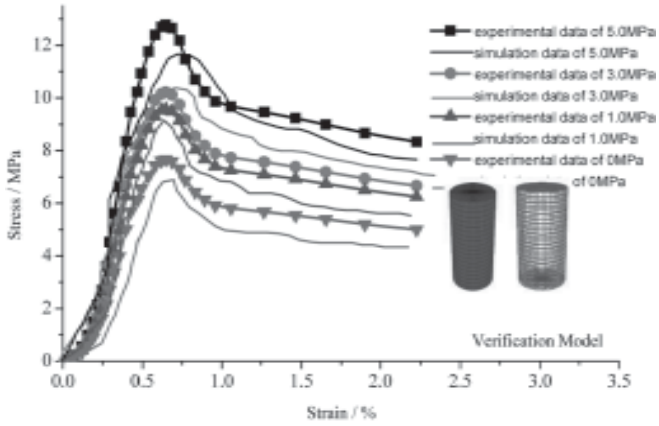


Fig.4 Model verification and analysis

It can be seen from Fig.4 that the strain-softening model with linear variation can well reflect the overall trend of the $\overline{c}$ deformation curve at the required accuracy.

## 4. Analysis of roadway support based on strain softening

4.1 Numerical model and parameters

According to the engineering conditions of the test coal mine, we built a numerical model of the roadway construction, as shown in Fig.5, with the size being 15m width 30m length and 30m height. For the rock, we adopted the strain-softening model proposed in this paper; we used cable units to simulate anchor bolts, shell units to simulate the reinforcing mesh and solid elements to simulate the U-shaped steel shed and shotcrete.

Parameters of the rock, anchor support and shotcrete are listed in Tables 3 and 4.

The initial stress is calculated by the elastic method and corrected according to the measured ground stress, and the vertical stress of the roadway floor is 6.72MPa (low stress test value is 6.38MPa), and the horizontal stress is 4.81MPa (low stress test value is 4.35MPa).

According to the construction design, the steps to simulate the excavation and supporting are: first for the upper excavation, run 100 steps to simulate the stress release process before the supporting; and second apply the upper bolt support; last after excavating the upper part for 15m, start the excavation of the lower part, and set up steel support and shotcrete support.

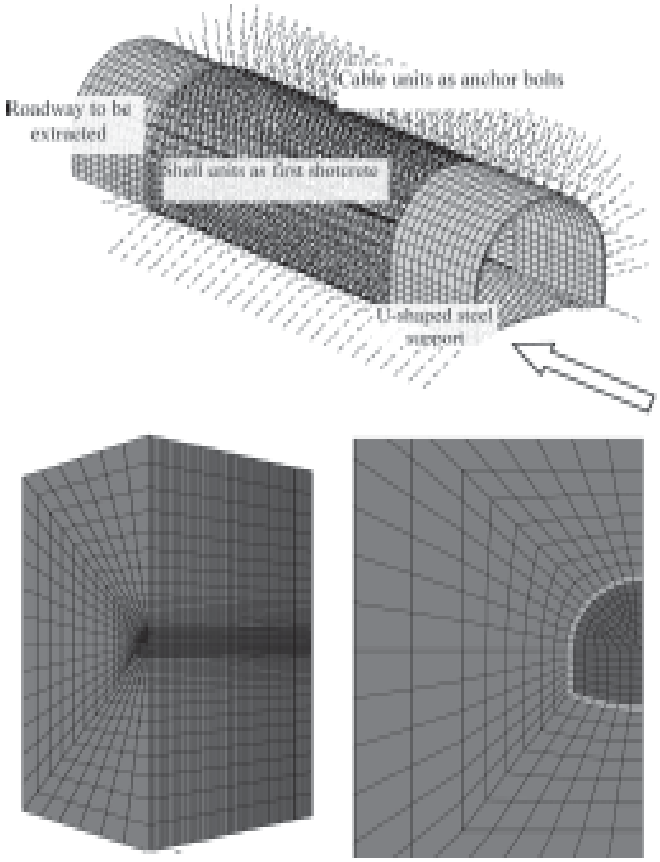


Fig.5 Roadway model diagram

### 4.2 Evaluation on surrounding rock failure

According to the analysis of the strain-softening constitutive relation in 3.1, the rock failure is related to the plastic shear strain and the minimum principal stress. Therefore, the stability of the surrounding rock can be measured by softening degree (SSD) of the surrounding rock [15-17], which can be determined using the following formula:

$$SSD = \begin{cases} \varepsilon^{ps} / \varepsilon^{pf} & \varepsilon^{ps} \le \varepsilon^{pf} \\ 1 & \varepsilon^{ps} > \varepsilon^{pf} \end{cases} \quad \ldots \quad (7)$$

where, $\varepsilon^{pf}$ is the finite limit plastic strain value of the rock, and $\varepsilon^{ps}$ is the corresponding strain value of the rock after stress change. SSD reflects the rock's proximity to the residual stress zone after the peak stress, with a range of $0 \le SSD \le 1$.

In FLAC3D, it is a little difficult to directly use the plastic strain to reflect SSD, but the variations in the internal cohesion and internal friction angle of the rock are linear to the plastic strain increment [18-20], meaning that the following equation holds:

$$\frac{\varepsilon^{ps}}{\varepsilon^{pf}} = \frac{C_0 - C}{C_0 - C^*} = \frac{\varphi_0 - \varphi}{\varphi_0 - \varphi^*} \quad \ldots \quad (8)$$

where, $C_0$ and $\varphi_0$ are the internal cohesion and internal friction angle of the rock; $C^*$ and $\phi^*$ are the internal cohesion and internal friction angle of the residual stress zone of the rock. $C_0$ and $\varphi_0$ can be calculated with the compression test envelopes under different confining pressures, and $C^*$ and $\phi^*$ can be obtained based on the molar stress circle envelopes in the residual stress phase.

The SSD determined by Formula (7) and (8) can be obtained through the fish programming in FLAC.

### 4.3 Analysis on the softening rule of the surrounding rock in soft rock roadway construction

According to the simulation results, the shear stress concentrated area after the upper part is excavated for 4.0m is shown in Fig.6, and the shear stress changes after the lower part is excavated for 4.0m are shown in Fig.7.

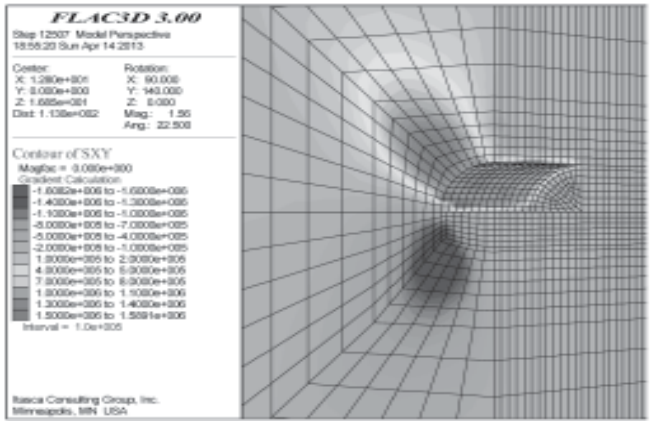


Fig.6 Shear stress distribution after upper excavation and supporting

Table 3: Parameters of rock and concrete

| Lithology | E | μ | $\sigma_t$ | C | $\varphi$ | * |
|---|---|---|---|---|---|---|
| | GPa | | MPa | MPa | (°) | (°) |
| Mudstone | 6.2 | 0.31 | 3.91 | * | * | 18 |
| Shotcrete | 28 | 0.26 | - | - | - | - |

Note: The cohesion and friction angle in the table are generalized cohesion and generalized friction angle.

Table 4: Paramters of Anchor Support

| Parameters | emod (Pa) | ytens (Pa) | gr_k (Pa) | gr_coh (Pa) | gr_fric (°) | xcarea ($m^2$) | gr_per (m) |
|---|---|---|---|---|---|---|---|
| Value | 2.0e11 | 3e9 | 6.5e8 | 3.6e3 | 24 | 3.8e-2 | 0.314 |

It can be seen from Fig.6 and Fig.7 that the maximum shear stress in the shear stress concentrated area after the lower excavation is increased obviously. According to the SSD calculation results, the maximum SSD and corresponding softening depths of the rock after the

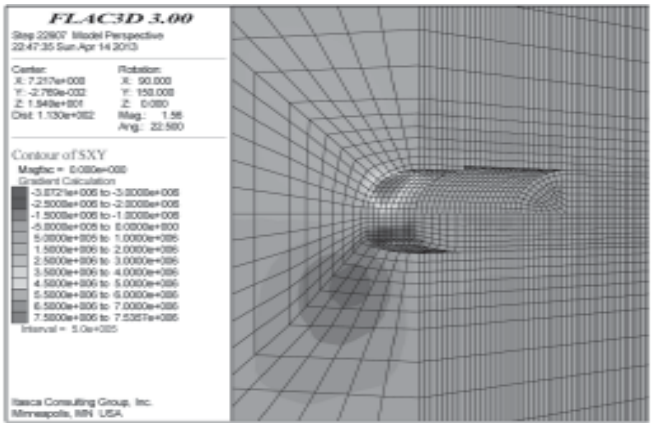


Fig.7 Shear stress concentrated area of lower excavation

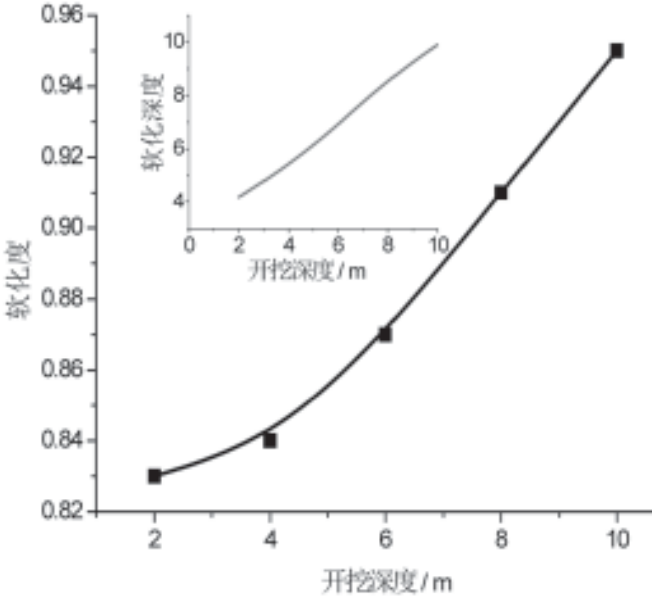


Fig.8 Change curve of SSD and softening depth associated with excavated depth

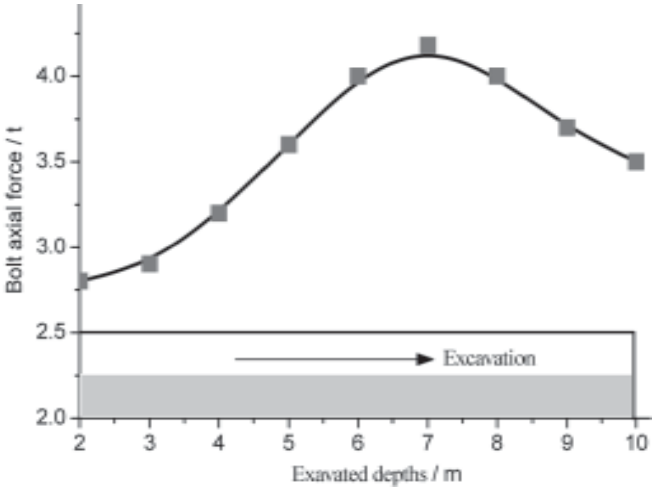


Fig.9 Changes in the axial force of the anchor bolts in spandrel

upper part is excavated for 2.0m, 4.0m, 6.0m, 8.0m and 10.0m are shown in Fig.8.

It can be seen from Fig.8 that with the increase of the excavated depth, the maximum SSD and softening depth of the surrounding rock are increasing, which also reflects that the supporting structure has no effect on the deformation control of the surrounding rock. According to the simulation results, changes in the axial force of the anchor bolts are shown in Fig.9.

It can be seen from Fig.9 that the maximum SSD and softening depth of the surrounding rock are increasing due to the stress concentration of the surrounding rock, and as a result, the anchoring force of the anchor bolts first increases gradually and then decreases.

## 5. Conclusions

In this paper, we take the typical weakly-cemented mudstone in Luxi coal mine in Inner Mongolia as the research object. We took samples on site, carried out an indoor triaxial compression test on the samples, analyzed the post-peak strain rule of the weakly-cemented mudstone and used the generalized cohesion and generalized friction angle model to analyze the stability of the roadway support. And the main conclusions are as follows:

(1) The triaxial compression test curve of the mudstone in the post-peak zone has an obvious strain-softening behaviour and there exists a residual stress zone. Therefore, the bi-linear strain-softening model in the FLAC is not suitable to describe the deformation process. The tri-linear strain-softening model is more suitable for analysis;

(2) The generalized internal cohesion and generalized internal friction angle are used to analyze the strength of mudstone. After curve fitting, it is found that the generalized internal cohesion and generalized internal friction angle are functionally related to the minimum principal stress and plastic shear strain. After being verified with fish programming, the model is more consistent with the deformation behaviour of the mudstone;

(3) Through the numerical simulation analysis of the mudstone roadway construction, and the evaluation on the SSD of the surrounding rock, it is found that the SSD and the softening depth of the mudstone roadway are not controlled by the shotcreting support, but rather increased, and the anchor bolt axial force is increased first and then reduced, reflecting that the anchor bolts have failed.

## References

1. Zhao, Z. H., Wang, W. M. and Wang, L. (2013): "Response models of weakly consolidated soft rock roadway under different interior pressures considering dilatancy effect," *Journal of Central South University*,

Vol. 20, No. 10, pp.3736-3744.

2. Wang, W. M., Zhao, Z. H. and Wang, L. (2013): "Elastic-plastic damage analysis for weakly consolidated surrounding rock regarding stiffness and strength cracking," *Journal of Mining & Safety Engineering*, Vol. 30, No. 5, pp: 679-685.
3. Yang, G. S., Tian, J. F. and Ye, W. J. (2014): "Influence of freeze-thaw cycles on Yangqu tunnel loess meso-damage evolution," *Journal of Xi'an University of Science and Technology*, Vol. 34, No. 6, pp. 635-640.
4. Zhang, H. M. and Yang, G. S. (2012): "Research on rock freeze-thaw cycle and anti-tensile characteristics test," *Journal of Xi'an University of Science and Technology*, Vol. 32, No.6, pp. 691-695.
5. Li, D. W., Wang, R. H. and Fan, J. H. (2010): "The deformation properties of mudstone and numerical calculation based on unloading path," *Journal of China Coal Society*, Vol. 35, No.10, pp. 1604-1608.
6. Li, D. W., Wang, R. H. and Fan, J. H. (2010): "The deformation properties of mudstone and numerical calculation based on unloading path," *Journal of China Coal Society*, Vol. 35, No. 3, pp. 387-391.
7. Lu, Y. L., Wang, L. G. and Yang, F. (2010): "Post-peak strain softening mechanical properties of weak rock," *Chinese Journal of Rock Mechanics and Engineering*, Vol. 29, No. 3, pp. 641-648.
8. Zhao, Z. H. and Wang W. M. (2013). "Deformation and Failure Behavior of Three-body Model Composed of Weak Rock and Strong Coal," *Electronic Journal of Geotechnical*, Vol. 28, No.R, pp. 3867-3880.
9. Liao, H. J., Ning, C. M. and Yu, M. H. (1998): "Experimental Study on Strength-deformation-time Relationship of soft Rock," *Rock and Soil Mechanics*, Vol. 19, No. 2, pp. 8-13.
10. Li, H. Z., Liao, H. J. and Kong, L. W. (2007): "Experimental study on stress-strain relationship of expansive mud-stone," *Rock and Soil Mechanics*, Vol. 28, No. 1, pp. 107-110.
11. Meng, Q. B., Han, L. J. and Qiao, W. G. (2012): "Mechanism of rock deformation and failure and monitoring analysis in water-rich soft rock roadway of western China," *Journal of Coal Science and Engineering (China)*, Vol. 18, No. 3, pp. 262-270.
12. Meng, Q. B., Han, L. J. and Qiao, W. G. (2014): "Support technology for mine roadways in extreme weakly cemented strata and its application," *International Journal of Mining Science and Technology*, Vol. 24, No. 2, pp. 157-164.
13. Li, W. T., Li, S. C. and Feng, X. D. (2011): "Study of post-peak strain softening mechanical properties of rock based on mohr-coulomb criterion," *Chinese Journal of Rock Mechanics and Engineering*, Vol. 30, No. 7, pp. 1460-1466.
14. Zhang, C. H., Zhao, Q. S. and Huang, L. (2010): "Post-peak strain softening mechanical model of rock considering confining pressure effect," *Rock and Soil Mechanics*, Vol. 31, No. S2, pp. 193-197.
15. Lee, Y. K. and Pietruszczak, S. (2008): "A new numerical procedure for elastoplastic analysis of a circular opening excavated in a strain-softening rock mass," *Tunnelling and Underground Space Technology*, Vol. 23, No.5, pp.588-599.
16. Aissa, A., Said, B., Mohamed, T. and Ahmed, B. (2015): "Numerical study of mixed convection in cylinrical czochralski configuration for crystal growth of silicon," *International Journal of Heat and Technology*, Vol. 33, NO. 1, pp.39-46. DOI:10.18280/ijht.330106.
17. Park, K. H., Tontavanich, B. and Lee, J. G. (2008). "A simple procedure for ground response curve of circular tunnel in elastic-strain softening rock masses," *Tunnelling and Underground Space Technology*, Vol. 23, No. 2, pp. 151-159.
18. He, M. C., Yuan, Y. and Wang, X. L. (2013): "Control technology for large deformation of mesozoic compound soft rock in xinjiang and its application," *Chinese Journal of Rock Mechanics and Engineering*, Vol. 32, No. 3, pp. 434-441.
19. Lv, S. J. and Feng, M. Q. (2015): "Three-dimensional numerical simulation of flow in Daliushu reach of the yellow river," *International Journal of Heat and Technology*, Vol. 33, No. 1, pp.107-114.
20. Han, J. X., Li, S. C. and Li, S. C. (2013): "Study of post-peak stress-strain relationship of rock material based on evolution of strength parameters," *Rock and Soil Mechanics*, Vol. 34, No. 2, pp.342-346.